DOI 10.59277/RoAJ.2025.1-2.03

SECULAR DYNAMICS AROUND ASTEROIDS WITH JOINT EFFECTS OF OBLATENESS AND THIRD BODY PERTURBATIONS

GABRIELA NADABAICA

Faculty of Matematics, Alexandru Ioan Cuza University of Iași,
Blvd. Carol I, No. 11, 700506 Iași, Romania
Email*: nadabaicagabriela@yahoo.com*

Abstract. This paper deals with long-term dynamics around asteroids. The orbital motion, perturbed by the oblateness of the central body and the attraction of the Sun, is studied both analytically and numerically. A simplified model, which takes into account the effects of the J_2 harmonic terms and the solar attraction and defined in terms of the Milankovitch variables, is used to analytically predict the evolution of the inclination and the longitude of the ascending node of circular orbits around asteroids. The key parameters, which lead to large variations of the orbital plane, are identified. In this sense, it is shown that the obliquity of the asteroid plays an important role. The analytical study is validated through numerical simulations, dealing with more complete models developed in both Cartesian and Hamiltonian frameworks. Due to the combined influence of the J_3 harmonic terms and secular solar resonances, although the orbital plane evolves as predicted by the analytical study, the initially circular orbits might become very eccentric. The methods are used to investigate the orbital stability around Vesta and Eros, respectively.

Key words: Dynamics around asteroids, orbital motions, oblateness effects, third body perturbations, long-term evolution of the orbital elements, equilibria, stability, chaotic motions.

1. INTRODUCTION

The investigation of orbital dynamics in the vicinity of irregularly shaped celestial bodies, such as asteroids, represents a complex and multifaceted problem in celestial mechanics. The non-spherical mass distribution of these bodies generates intricate gravitational fields, which increase in complexity when external perturbations from the Sun and other massive bodies within the solar system become relevant. Asteroids, such as Vesta and Eros, with their distinct physical and dynamical characteristics, serve as appropriate cases for studying the dynamical interaction with these complex gravitational fields. Vesta, one of the largest bodies in the asteroid belt, exhibits a relatively massive and oblate shape. The Vesta's equatorial plane is tilted by 27° from its orbital plane. Conversely, Eros, a smaller and more irregularly shaped near-Earth asteroid, displays pronounced asymmetries in its mass distribution, and the obliquity if very large, about 89°.

The purpose of this paper is to show that the obliquity of the asteroid plays a critical role in shaping the orbital dynamics, with Vesta's moderate obliquity (27°) fostering more stable regions compared to Eros's high obliquity (89°), which leads to larger excursions in inclination and chaotic behavior. Numerical simulations validate the analytical results, demonstrating the impact of higher–order harmonics (J_3) and solar secular resonances on orbital stability. These insights contribute to a deeper understanding of the dynamical environments around irregularly shaped asteroids, offering valuable implications for future asteroid missions, the study of solar system dynamics, and the broader field of celestial mechanics.

2. MODELS

2.1. PRELIMINARIES

We consider an infinitesimal particle (a massless natural or artificial satellite), hereafter denoted as P, orbiting an asteroid that itself follows a Keplerian orbit around the Sun and rotates uniformly about a fixed axis. The massless body P experiences gravitational forces from the oblate asteroid, as well as from the Sun. We neglect all other external forces in this analysis.

The orbital motion of the massless body P is referred to a quasi–inertial frame $\mathbf{R}_A^e = \{A; \mathbf{e}_1, \mathbf{e}_2, \mathbf{e}_3\}$, centered in the center of mass A of the asteroid, where $\mathbf{e}_3$ is the unit vector normal to the equatorial plane of the asteroid and oriented toward the positive pole of rotation (that is the pole given by the right–hand rule for the rotational motion, see Archinal *et al.* (2011) for more details), the unit vectors $\mathbf{e}_1$ and $\mathbf{e}_2$ are in the equatorial plane of the asteroid and defined as $\mathbf{e}_1 = \frac{\mathbf{e}_3 \times \mathbf{n}}{|\mathbf{e}_3 \times \mathbf{n}|}$ and $\mathbf{e}_2 = \mathbf{e}_3 \times \mathbf{e}_1$, respectively, where $\mathbf{n}$ is the unit vector normal to the ecliptic plane and pointing towards the north ecliptic plane.

Let us introduce another reference frame, a body frame fixed to the asteroid, denoted by $\mathbf{R}_A^f = \{A; \mathbf{f}_1, \mathbf{f}_2, \mathbf{f}_3\}$, where $\mathbf{f}_1$ and $\mathbf{f}_2$ are in the equatorial plane of the asteroid, $\mathbf{f}_3 = \mathbf{e}_3$ is directed along the rotation axis, while $\mathbf{f}_1$ is in the plane of the prime meridian of the asteroid (see Archinal *et al.* (2011) for the location of prime meridian of various asteroids). The rotational motion of the asteroid is described by the angle θ between $\mathbf{e}_1$ and $\mathbf{f}_1$, namely

$$\theta(t) = \dot{\theta} t + \theta_0, \tag{1}$$

where $\dot{\theta}$ and θ_0, with $\theta_0 = \theta(t_0)$ at a given epoch t_0, are known.

Denoting by $\mathbf{r}$ the position vector of the satellite P with coordinates (x, y, z) in the quasi–inertial frame $\mathbf{R}_A^e$ and (X, Y, Z) in the synodic frame $\mathbf{R}_A^f$:

$$\mathbf{r} = x\mathbf{e}_1 + y\mathbf{e}_2 + z\mathbf{e}_3 = X\mathbf{f}_1 + Y\mathbf{f}_2 + Z\mathbf{f}_3 \; .$$

The relation between the coordinates in the two frames is given by:

$$\begin{pmatrix} X \\ Y \\ Z \end{pmatrix} = \begin{pmatrix} \cos\theta & \sin\theta & 0 \\ -\sin\theta & \cos\theta & 0 \\ 0 & 0 & 1 \end{pmatrix} \begin{pmatrix} x \\ y \\ z \end{pmatrix} \equiv R_3(-\theta) \begin{pmatrix} x \\ y \\ z \end{pmatrix}, \qquad (2)$$

where $R_3(\theta)$ denotes the rotation matrix of angle θ around the third axis.

Let us assume that the orbital motion of the asteroid around the Sun is Keplerian. And let the orbital elements of the asteroid with respect to the ecliptic plane be $(a_A, e_A, i_A, M_A, \omega_A, \Omega_A)$, where a_A is the semi–major axis, e_A is the eccentricity, i_A is the inclination, M_A is the mean anomaly, ω_A is the argument of perihelion, and Ω_A is the longitude of the ascending node. As a consequence, the motion of the Sun with respect to the asteroid is also Keplerian. The Sun's motion with respect to the reference frame $\mathbf{R}_A^e$ is characterized by the orbital elements $(a_S^*, e_S^*, i_S^*, M_S^*, \omega_S^*, \Omega_S^*)$. These are related to the orbital elements of the asteroid through

$$a_S^* = a_A, \qquad e_S^* = e_A, \qquad (3)$$

and some formulas for rotation (see Galeş *et al.* (2025) for details):

$$\begin{aligned} &\cos i_S^* = \cos i_A \sin\beta - \sin i_A \cos\beta \sin(\lambda - \Omega_A), \\ &\sin i_S^* \cos\Omega_S^* = \cos i_A \cos\beta + \sin i_A \sin\beta \sin(\lambda - \Omega_A), \\ &\sin i_S^* \sin\Omega^* = \sin i_A \cos(\lambda - \Omega_A), \\ &\sin i_S^* \cos(\omega_S^* + \omega_A) = \sin\beta \sin i_A + \cos\beta \cos i_A \sin(\lambda - \Omega_A), \\ &\sin i_S^* \sin(\omega_S^* + \omega_A) = \cos\beta \cos(\lambda - \Omega_A), \end{aligned} \qquad (4)$$

where β and λ are the ecliptic latitude and the ecliptic longitude, respectively, of the positive pole of rotation of the asteroid. We assume that β, λ, and the orbital elements of the asteroid are known. Then, in view of (3) and (4) the orbital elements of the Sun are uniquely determined.

2.2. THE MODEL IN THE CARTESIAN FRAMEWORK

The motion of the satellite P is described by equations that account for the combined gravitational influence of the asteroid, including the oblateness effect, and the solar attraction. Other contributions, which are neglected in this case. Within the asteroid–centered frame $\mathbf{R}_A^e$, the motion of P is described by the equation

$$\ddot{\mathbf{r}} = -\mathcal{G} \int_{V_O} \rho(\mathbf{r}_p) \frac{\mathbf{r} - \mathbf{r}_p}{|\mathbf{r} - \mathbf{r}_p|^3} dV_O - \mathcal{G} m_S \Big(\frac{\mathbf{r} - \mathbf{r}_S}{|\mathbf{r} - \mathbf{r}_S|^3} + \frac{\mathbf{r}_S}{|\mathbf{r}_S|^3} \Big), \qquad (5)$$

where $\mathcal{G}$ is the gravitational constant, $\rho(\mathbf{r}_p)$ is the density at some point $\mathbf{r}_p$ inside the volume V_O of the asteroid, m_S is the mass of the Sun, $\mathbf{r}_S$ is the position vector of the Sun with respect to the center A of the asteroid.

Let us denote by ∇_F and ∇_I the gradients in the synodic and quasi-inertial frames:

$$\begin{aligned} \nabla_F &\equiv \frac{\partial}{\partial X}\mathbf{f}_1 + \frac{\partial}{\partial Y}\mathbf{f}_2 + \frac{\partial}{\partial Z}\mathbf{f}_3, \\ \nabla_I &\equiv \frac{\partial}{\partial x}\mathbf{e}_1 + \frac{\partial}{\partial y}\mathbf{e}_2 + \frac{\partial}{\partial z}\mathbf{e}_3. \end{aligned} \tag{6}$$

The relation (5) can be written in the form

$$\ddot{\mathbf{r}} = -R_3(\theta)\nabla_F V(\mathbf{r}) + Gm_S \nabla_I \Big(\frac{1}{|\mathbf{r}-\mathbf{r}_S|} - \frac{\mathbf{r}\cdot\mathbf{r}_S}{|\mathbf{r}_S|^3} \Big), \tag{7}$$

where the gravitational potential due to the oblate body is given by

$$V(\mathbf{r}) = -\mathcal{G}\int_{V_O} \frac{\rho(\mathbf{r}_p)}{|\mathbf{r}-\mathbf{r}_p|} dV_O. \tag{8}$$

In the synodic frame we can write

$$X = r\cos\phi\cos\chi, \qquad Y = r\cos\phi\sin\chi, \qquad Z = r\sin\phi, \tag{9}$$

where (r,χ,ϕ) are spherical coordinates with the longitude $0 \le \chi \le 2\pi$ and the latitude $-\frac{\pi}{2} \le \phi \le \frac{\pi}{2}$. Let m_0 represent the mass and R_0 denote a reference radius (such as the equatorial or equivalent radius) of the asteroid. The gravitational potential V can be expanded in terms of spherical harmonics as follows (see Kaula, 1961, 1966):

$$V(r,\phi,\chi) = -\frac{\mathcal{G}m_0}{r}\sum_{n=0}^{\infty}\Big(\frac{R_0}{r}\Big)^n \sum_{m=0}^{n} P_{nm}(\sin\phi)(C_{nm}\cos m\chi + S_{nm}\sin m\chi), \tag{10}$$

where the quantities P_{nm} are defined in terms of the Legendre polynomials:

$$P_n(x) \equiv \frac{1}{2^n n!}\frac{d^n}{dx^n}\{(x^2-1)^n\}, \qquad P_{nm}(x) \equiv (1-x^2)^{\frac{m}{2}}\frac{d^m}{dx^m}\{P_n(x)\},$$

and C_{nm}, S_{nm}, with $n,m \in \mathbb{N}$ and $0 \le m \le n$, are the un-normalized spherical harmonic coefficients. We recall that the un–normalized coefficients C_{nm}, S_{nm} are related to the normalized spherical harmonic coefficients $\overline{C}_{nm}$, $\overline{S}_{nm}$ as follows: $(\overline{C}_{nm}, \overline{S}_{nm}) = N_{nm}(C_{nm}, S_{nm})$, where the normalization factor N_{nm} is defined as:

$$N_{nm} = \sqrt{\frac{(2-\delta_{0m})(2n+1)!(n-m)!}{(n+m)!}},$$

with δ_{0m} denoting the Kronecker delta.

Since V is expanded in power series of R_0/r, the magnitude of the harmonic terms decreases with the increase of n and the increase in distance r from the asteroid. This work assumes that the harmonic coefficients C_{nm} and S_{nm}, with $0 \le m \le n \le n_{max}$, where $n_{max} = 4$, are known. Tables1 and 2 provide the values of the

Table 1

Vesta's harmonic coefficients $\overline{C}_{nm}$, $\overline{S}_{nm}$, C_{nm}, S_{nm}, J_{nm}, expressed at a reference radius $R_0 = 265\,[km]$ (see Konopliv *et al.*, 2017) and the quantities χ_{nm}

n	m	$\overline{C}_{nm}$	$\overline{S}_{nm}$	C_{nm}	S_{nm}	J_{nm}	χ_{nm}
2	0	–3.17794e-02	0.00000e+00	–7.10608e-02	0.00000e+00	7.10608e-02	
2	1	–4.93914e-10	1.59604e-09	–6.37640e-10	2.06049e-09	2.15689e-09	$287\overset{\circ}{.}19$
2	2	4.18496e-03	1.24537e-03	2.70138e-03	8.03888e-04	2.81845e-03	$98\overset{\circ}{.}28$
3	0	3.31055e-03	0.00000e+00	8.75890e-03	0.00000e+00	–8.75890e-03	
3	1	–2.61267e-03	–4.33891e-04	–2.82200e-03	–4.68656e-04	2.86065e-03	$9\overset{\circ}{.}42$
3	2	–7.28890e-04	–1.17304e-03	–2.48963e-04	–4.00670e-04	4.71720e-04	$29\overset{\circ}{.}07$
3	3	–1.54662e-04	2.38493e-03	–2.15666e-05	3.32563e-04	3.33262e-04	$331\overset{\circ}{.}23$
4	0	3.26560e-03	0.00000e+00	9.79680e-03	0.00000e+00	–9.79680e-03	
4	1	4.92039e-04	1.43488e-04	4.66789e-04	1.36125e-04	4.86233e-04	$196\overset{\circ}{.}25$
4	2	–6.30098e-04	2.63033e-04	–1.40894e-04	5.88159e-05	1.52677e-04	$348\overset{\circ}{.}67$
4	3	–1.04752e-04	–6.69982e-04	-6.26017e-06	–4.00390e-05	4.05255e-05	$27\overset{\circ}{.}03$
4	4	8.66352e-05	–2.97036e-04	1.83050e-06	–6.27605e-06	6.53754e-06	$26\overset{\circ}{.}56$

normalized and un–normalized harmonic coefficients up to degree and order $n = m = n_{max}$ for the asteroids (4) Vesta and (433) Eros, determined for a specific radius R_0. The tables also include the values of the un–normalized coefficients J_n, J_{nm} and the values of the angles χ_{nm}, for $n, m \in \mathbb{N}$ and $0 < m \leq n$, defined through the relations

$$\begin{aligned} &J_n \equiv J_{n0} = -C_{n0}\,, \\ &C_{nm} = -J_{nm}\cos(m\chi_{nm})\,, \qquad S_{nm} = -J_{nm}\sin(m\chi_{nm})\,, \qquad \text{for } m > 0. \end{aligned} \tag{11}$$

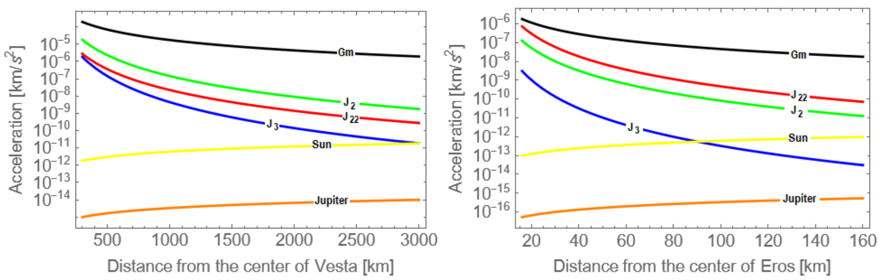

Fig. 1 – Order of magnitude of different perturbations as a function of the distance from the center of the oblate body. In the left panel: 4 Vesta, in the right panel: 433 Eros. The colored curves show the influence of: the monopole term of the gravitational influence of the minor body (black), J_2 (green), J_{22} (red), J_3 (blue), the attraction of the Sun (yellow) and Jupiter (orange).

Using (9), the series of V, given by the relation (10), can be expressed as a function of the Cartesian coordinates X, Y and Z, namely $V = V(X,Y,Z)$. Calculating the gradient $\nabla_F V$, multiplying the resulting vector by $\mathcal{R}_3(\theta)$ and using the relation (2), we can express the first term of equation (7) in terms of the coordinates

Table 2

Eros's harmonic coefficients $\overline{C}_{nm}$, $\overline{S}_{nm}$, C_{nm}, S_{nm}, J_{nm}, expressed at a reference radius $R_0 = 16\,[km]$ (see Miller *et al.*., 2002) and the quantities χ_{nm}

n	m	$\overline{C}_{nm}$	$\overline{S}_{nm}$	C_{nm}	S_{nm}	J_{nm}	χ_{nm}
2	0	–2.34688e-02	0.00000e+00	–5.24780e-02	0.00000e+00	5.24780e-02	
2	1	0.00000e+00	0.00000e+00	0.00000e+00	0.00000e+00	0.00000e+00	
2	2	1.27867e-01	–4.29823e-02	8.25380e-02	–2.77450e-02	8.70764e-02	$80^\circ\!.71$
3	0	–5.29150e-04	0.00000e+00	–1.40000e-03	0.00000e+00	1.40000e-03	
3	1	3.75420e-03	3.12834e-03	4.05500e-03	3.37900e-03	5.27832e-03	$219^\circ\!.80$
3	2	5.24643e-03	–2.00840e-03	1.79200e-03	-6.86000e-04	1.91881e-03	$79^\circ\!.52$
3	3	–7.41304e-02	-8.70174e-02	–1.03370e-02	–1.21340e-02	1.59401e-02	$16^\circ\!.52$
4	0	4.30000e-03	0.00000e+00	1.29000e-02	0.00000e+00	–1.29000e-02	
4	1	–1.11733e-04	1.43356e-04	–1.06000e-04	1.36000e-04	1.72429e-04	$307^\circ\!.93$
4	2	–7.82400e-02	2.03124e-02	–1.74950e-02	4.54200e-03	1.80749e-02	$352^\circ\!.72$
4	3	–5.33789e-03	–2.35938e-03	-3.19000e-04	–1.41000e-04	3.48772e-04	$7^\circ\!.94$
4	4	8.32368e-01	–4.23070e-01	1.75870e-02	-8.93900e-03	1.97283e-02	$38^\circ\!.26$

x, y and z of the quasi-inertial frame $\mathbf{R}_A^e$. We obtain the following equations of motion:

$$\ddot{x} = -\frac{\mathcal{G}m_0\,x}{r^3} + \sum_{n=2}^{n_{max}}\sum_{m=0}^{n} f_{nm}^x(x,y,z,\theta) - \mathcal{G}m_S\Big(\frac{x-x_S}{|\mathbf{r}-\mathbf{r}_S|^3} + \frac{x_S}{r_S^3}\Big),$$
$$\ddot{y} = -\frac{\mathcal{G}m_0\,y}{r^3} + \sum_{n=2}^{n_{max}}\sum_{m=0}^{n} f_{nm}^y(x,y,z,\theta) - \mathcal{G}m_S\Big(\frac{y-y_S}{|\mathbf{r}-\mathbf{r}_S|^3} + \frac{y_S}{r_S^3}\Big),$$
$$\ddot{z} = -\frac{\mathcal{G}m_0\,z}{r^3} + \sum_{n=2}^{n_{max}}\sum_{m=0}^{n} f_{nm}^z(x,y,z,\theta) - \mathcal{G}m_S\Big(\frac{z-z_S}{|\mathbf{r}-\mathbf{r}_S|^3} + \frac{z_S}{r_S^3}\Big),$$

where the functions f_{nm}^x, f_{nm}^y and f_{nm}^z can be explicitly computed for any n and m. For example, f_{43}^x, f_{43}^y and f_{43}^z are given by

$$\begin{aligned} f_{22}^x(x,y,z,\theta) &= \frac{\mathcal{G}m_0R_0^2}{r^5}\Big\{6C_{22}^\theta x + 6S_{22}^\theta y + \frac{15x}{r^2}[C_{22}^\theta(y^2-x^2) - 2xyS_{22}^\theta]\Big\},\\ f_{22}^y(x,y,z,\theta) &= \frac{\mathcal{G}m_0R_0^2}{r^5}\Big\{6S_{22}^\theta x - 6C_{22}^\theta y + \frac{15y}{r^2}[C_{22}^\theta(y^2-x^2) - 2xyS_{22}^\theta]\Big\},\\ f_{22}^z(x,y,z,\theta) &= \frac{\mathcal{G}m_0R_0^2}{r^5}\Big\{\frac{15z}{r^2}[C_{22}^\theta(y^2-x^2) - 2xyS_{22}^\theta]\Big\}, \end{aligned} \tag{12}$$

where

$$\begin{pmatrix} C_{22}^\theta \\ S_{22}^\theta \end{pmatrix} = \begin{pmatrix} \cos 2\theta & -\sin 2\theta \\ \sin 2\theta & \cos 2\theta \end{pmatrix}\begin{pmatrix} C_{22} \\ S_{22} \end{pmatrix} \equiv \mathcal{R}^{2D}(2\theta)\begin{pmatrix} C_{22} \\ S_{22} \end{pmatrix} \tag{13}$$

and $\mathcal{R}^{2D}(\theta)$ is the rotation matrix of angle θ in two dimensions.

Figure 1 compares the relative strengths of different forces acting on a satellite orbiting Vesta and Eros. These include the monopole term of the gravitational influence from the oblate body (black), the body's oblateness with contributions from the coefficients J_2 (green), J_{22} (red), J_3 (blue), as well as the gravitational forces from the Sun (yellow) and Jupiter (orange). Clearly, the perturbing effects induced by Jupiter are negligible, so they are neglected in this study.

2.3. HAMILTONIAN FORMULATION

The Hamiltonian formulation provides a powerful framework for analyzing the long-term evolution of perturbed orbits. By expressing the gravitational potential in terms of action-angle variables, we can isolate secular and resonant terms that influence orbital dynamics (Brouwer and Clemence, 1961). This approach allows us to identify regions of stability and chaos, as well as critical resonances that govern the behavior of particles in the system (Murray and Dermott, 1999). In addition, the Hamiltonian approach is less expensive in computations.

When studying the evolution of the orbit over time, it is more practical to represent it in terms of the orbital elements $\Upsilon = (a, e, i, M, \omega, \Omega)$ of the satellite P, where a is the semi-major axis, e – the eccentricity, i – the inclination, M – the mean anomaly, ω – the argument of pericentre, Ω – the longitude of the ascending node. In terms of the orbital elements Υ, the potential (10) becomes:

$$V = -\frac{\mathcal{G}m_0}{r} - \frac{\mathcal{G}m_0}{a}\sum_{n=2}^{\infty}\sum_{m=0}^{n}\left(\frac{R_0}{a}\right)^n J_{nm}\sum_{p=0}^{n}F_{nmp}(i)\sum_{q=-\infty}^{\infty}G_{npq}(e)S_{nmpq}(M,\omega,\Omega,\theta)\,, \tag{14}$$

where F_{nmp} is the inclination function, G_{npq} is the eccentricity function and S_{nmpq} is the trigonometric function (see Kaula, 1966, for detailed definitions). The values of J_{nm} and χ_{nm}, up to degree and order 4, are given in Tables 1, 2 for the asteroids (4) Vesta and (433) Eros.

The solar disturbing function can be expressed in orbital elements as (see Kaula, 1962):

$$\begin{aligned}\mathcal{R}_{Sun} = \mathcal{G}m_S\sum_{l=2}^{\infty}\sum_{m=0}^{l}\sum_{p=0}^{l}\sum_{h=0}^{l}\sum_{q=-\infty}^{\infty}\sum_{j=-\infty}^{\infty}\frac{a^l}{(a_S^*)^{l+1}}\epsilon_m\frac{(l-m)!}{(l+m)!}\\ \times\mathcal{F}_{lmph}(i,i_S^*)\mathcal{H}_{lpq}(e)\mathcal{G}_{lhj}(e_S^*)\cos(\varphi_{lmphqj}),\end{aligned} \tag{15}$$

where

$$\mathcal{F}_{lmph}(i,i_S^*) \equiv F_{lmp}(i)F_{lmh}(i_S^*),$$
$$\varphi_{lmphqj} \equiv (l-2p)\omega + (l-2p+q)M - (l-2h)\omega_S^* - (l-2h+j)M_S^* + m(\Omega - \Omega_S^*),$$

with the quantities ϵ_m defined as

$$\epsilon_m = \begin{cases} 1, \text{ if } m = 0, \\ 2, \text{ if } m \in \mathbb{Z}^*. \end{cases}$$

The functions $\mathcal{H}_{lpq}(e)$ and $\mathcal{G}_{lhj}(e_S^*)$ are the Hansen coefficients $X_{l-2p+q}^{l,l-2p}(e)$ and $X_{l-2h+j}^{-(l+1),l-2h}(e_S^*)$, respectively (see Giacaglia (1976)).

Since the orbital elements are non-canonical variables, we use the Delaunay elements (L,G,H,M,ω,Ω), defined in terms of the orbital elements $\Upsilon = (a,e,i,M,\omega,\Omega)$ through the relations

$$L = \sqrt{\mu_0 a}\,, \qquad G = L\sqrt{1-e^2}\,, \qquad H = G\cos i\,, \tag{16}$$

where $\mu_0 = \mathcal{G}m_0$. The corresponding Hamiltonian has the form:

$$\mathcal{H} = -\frac{\mu_0^2}{2L^2} + \mathcal{H}_0(\Upsilon,\theta) + \mathcal{H}_{Sun}(\Upsilon,\Upsilon_S), \tag{17}$$

where the perturbations caused by the oblate body and the Sun are

$$\mathcal{H}_0 = V + \frac{\mu_0}{r}\,, \qquad \mathcal{H}_{Sun} = -\mathcal{R}_{Sun}\,, \tag{18}$$

θ is the rotation angle and $\Upsilon_S = (a_S^*, e_S^*, i_S^*, M_S^*, \omega_S^*, \Omega_S^*)$ the orbital elements of the Sun.

The associated canonical equations are:

$$\begin{aligned} \dot{M} &= \frac{\partial \mathcal{H}}{\partial L}\,, & \dot{L} &= -\frac{\partial \mathcal{H}}{\partial M}, \\ \dot{\omega} &= \frac{\partial \mathcal{H}}{\partial G}\,, & \dot{G} &= -\frac{\partial \mathcal{H}}{\partial \omega}, \\ \dot{\Omega} &= \frac{\partial \mathcal{H}}{\partial H}\,, & \dot{H} &= -\frac{\partial \mathcal{H}}{\partial \Omega}. \end{aligned}$$

The series expansions in equations (14) and (15) contain an infinite number of terms, generated by a multitude of possible combinations of angles in the argument of the trigonometric functions. Among these terms, only a subset is significant for the study of the dynamics of the infinitesimal body. According to the principle of averaging, short-period terms are negligible if the analysis is conducted over a sufficiently long timescale. Therefore, in orbit propagation, we shall average the Hamiltonian (17) over the mean anomaly M and take the expansion of $\mathcal{H}_0$ up to degree $n = 4$, while the expansion $\mathcal{H}_{Sun}$ up to $l = 2$. Although the resulted Hamiltonian provides the evolution of the mean orbital elements rather than the osculating orbital elements, on long-time scales, these elements describe the orbital evolution.

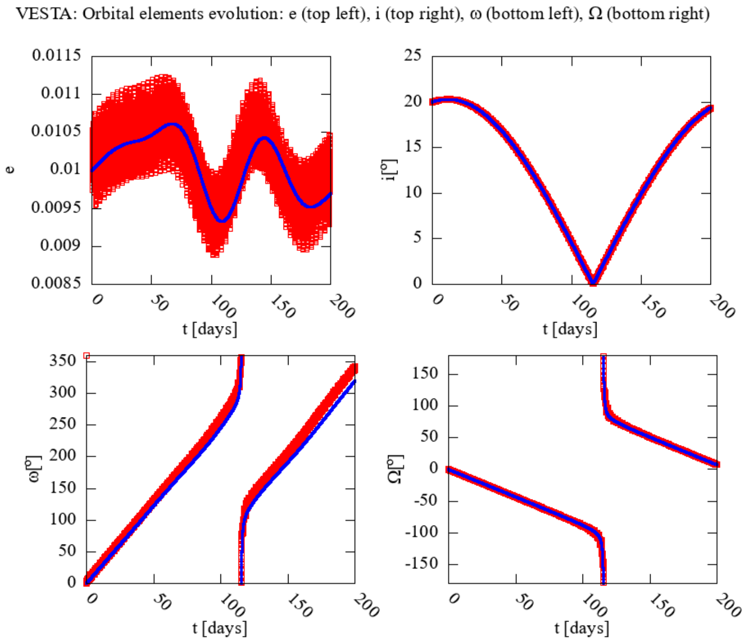

Fig. 2 – Comparison between the Cartesian model (in red) and the Hamiltonian model (in blue). The evolution of the orbital elements up to 200 years.

Figure 2 compares the Cartesian (in red) and Hamiltonian (in blue) formulations for an orbit around Vesta. The initial conditions are $a(0) = 9000$ km, $e(0) = 0.1$, $i(0) = 20°$, $\omega(0) = 0°$, $\Omega(0) = 0°$ and the time span is 200 years. The orbital dynamics is clearly depicted by mean orbital elements.

2.4. MILANKOVITCH ELEMENTS

Figure 1 shows that in the close vicinity of the central body the main perturbation that influences the orbital motion of the satellite P is the asteroid's oblateness, while at increasingly larger distances from A, the attraction of the Sun becomes increasingly relevant. Since all J_{22} terms are short periodic for far orbits from the asteroid's surface, in these orbital regimes the main perturbing effects are due to J_2 and the Sun.

Therefore, to analyze the long-term behavior of distant orbits, we shall use a double-averaged model, in which the perturbing functions are averaged over both the mean anomaly of the satellite and the mean anomaly of the Sun, and in which the only perturbations are due to J_2 and the Sun. We shall use Milankovitch elements (see Milankovitch, 1939) because for the considered model, this formulation allows us to obtain some analytical results that characterize the evolution of the orbital elements.

The model in question is obtained as follows. First, we notice that by retaining only the perturbations due to J_2 and the attraction of the Sun, the equation of motion (5) reduces to

$$\ddot{\mathbf{r}} + \frac{\mu_0}{r^3}\mathbf{r} = \nabla_I U\,, \tag{19}$$

where $\mu_0 = \mathcal{G}m_0$, $\mu_S = \mathcal{G}m_S$ and U is the disturbing function

$$U = -\frac{\mu_0 R_0^2 J_2}{r^3}\Big(\frac{3}{2}\frac{z^2}{r^2} - \frac{1}{2}\Big) + \mu_S\Big(\frac{1}{|\mathbf{r}-\mathbf{r_S}|} - \frac{\mathbf{r}\cdot\mathbf{r_S}}{|\mathbf{r}_S|^2}\Big)\,. \tag{20}$$

Since $r \ll r_S$, we only keep the terms up to degree $l = 2$ in the following expansion

$$\frac{1}{|\mathbf{r}-\mathbf{r}_S|} = \frac{1}{|\mathbf{r}_S|}\sum_{l=0}^{\infty}\left(\frac{|\mathbf{r}|}{|\mathbf{r}_S|}\right)^l P_l(\cos\Theta)\,,$$

where Θ is the angle between $\mathbf{r}$ and $\mathbf{r}_S$ and P_l are the Legendre polynomials.

Then, taking the average over the mean anomaly of the satellite and the mean anomaly of the Sun, we deduce that the doubly-averaged disturbing function has the form (see Allan and Cook (1964) for more details)

$$U = na^2 U^*, \tag{21}$$

with

$$\begin{aligned} U^* = {} & \frac{\omega_0}{(1-e^2)^{3/2}}\left(\frac{1}{2}(\mathbf{R}\cdot\mathbf{R}_A)^2 - \frac{1}{6}\right) \\ & + \omega_1\left(\frac{1}{2}(1-e^2)(\mathbf{R}\cdot\mathbf{R}_S)^2 + e^2\Big(1 - \frac{5}{2}(\mathbf{P}\cdot\mathbf{R}_S)^2\Big)\right), \end{aligned} \tag{22}$$

where n is the mean motion of the particle and

$$\omega_0 = \frac{3nJ_2R_0^2}{2a^2}, \qquad \omega_1 = \frac{3\mu_S}{4na_S^3(1-e_S^2)^{3/2}}. \tag{23}$$

In (22), the unit vectors $\mathbf{R}$ and $\mathbf{P}$ correspond to the particle's orbit, namely $\mathbf{R}$ is the positive normal of the orbital plane, while $\mathbf{P}$ belongs to the orbital plane and points in the direction of the pericenter. The unit vector $\mathbf{R}_A$ is directed along the rotation axis of the asteroid, namely $\mathbf{R}_A = \mathbf{e}_3 = \mathbf{f}_3$ (see Section 2.1), and the unit vector $\mathbf{R}_S$ is normal to the orbital plane of the Sun.

Finally, by taking the vectorial elements $\mathbf{e}$ and $\mathbf{h}$ defined by

$$\mathbf{e} = e\mathbf{P}, \qquad \mathbf{h} = (1-e^2)^{1/2}\mathbf{R}, \tag{24}$$

the evolution of the orbital elements is described by the equations (see Allan and Cook, 1964):

$$\dot{\mathbf{h}} = \mathbf{h}\times\frac{\partial U^*}{\partial\mathbf{h}} + \mathbf{e}\times\frac{\partial U^*}{\partial\mathbf{e}}\,, \qquad \dot{\mathbf{e}} = \mathbf{e}\times\frac{\partial U^*}{\partial\mathbf{h}} + \mathbf{h}\times\frac{\partial U^*}{\partial\mathbf{e}}\,. \tag{25}$$

The disturbing function U^* can be expressed in terms of the vectorial elements $\mathbf{h}$ and $\mathbf{e}$ as

$$\begin{aligned} U^* =& \omega_0 \Big(\frac{1}{2}(1-e^2)^{-5/2} (\mathbf{h}\cdot\mathbf{R}_A)^2 - \frac{1}{6}(1-e^2)^{-3/2} \Big) \\ &+ \omega_1 \left(\frac{1}{2}(\mathbf{h}\cdot\mathbf{R}_S)^2 + e^2 - \frac{5}{2}(\mathbf{e}\cdot\mathbf{R}_S)^2 \right). \end{aligned} \tag{26}$$

3. LONG-TERM VARIATION OF THE INCLINATION OF CIRCULAR ORBITS

Following the work of Allan and Cook (1964), who investigated the dynamics of distant circular orbits of Earth's satellites, we analyze the long-term evolution of the inclination of the orbits around asteroids. We adopt an analytical framework to identify the key parameters that lead to large variation of the inclination of circular orbits.

In this study, the regions of interest include the orbits whose semi-major axis is larger than $8R_0$ and smaller than the Laplace radius of the sphere of influence $d_L = \rho_0 \left(\frac{m_0}{m_S}\right)^{2/5}$, where ρ_0 is the heliocentric distance of the asteroid. The sphere of influence is a region surrounding a celestial body, where the body exerts the main gravitational influence on an orbiting satellite, despite the presence of the much more massive but distant Sun. The concept of sphere of influence was recently revisited by Cavallari *et al.* (2023).

For the considered asteroids, the region of interest includes the orbits whose semi-major axis is between 2 100 km and 39 000 km, in the case of Vesta and, respectively, between 130 km and 360 km in the case of Eros. In such a region, the main disturbing effects are due to J_2 and the attraction of the Sun. Therefore, the simplified model described in Section 2.4 provides a good preliminary (analytical) overview of secular dynamics.

Because $\frac{\partial U^*}{\partial \mathbf{e}} = \mathbf{0}$ if the eccentricity $e = 0$ (see equation (26)), the second equation of (25) has the solution $\mathbf{e}(t) = 0$ for the initial condition $e(0) = 0$. Therefore, the initially circular orbits remain circular over time. In this case, the system of equations (25) reduces to a one degrees-of-freedom (integrable) problem characterized by the equation

$$\dot{\mathbf{R}} = -\omega_0(\mathbf{R}\cdot\mathbf{R}_A)(\mathbf{R}_A\times\mathbf{R}) - \omega_1(\mathbf{R}\cdot\mathbf{R}_S)(\mathbf{R}_S\times\mathbf{R}), \tag{27}$$

where the signification of the constants ω_0 and ω_1, as well as of the vectors $\mathbf{R}$, $\mathbf{R_A}$ and $\mathbf{R_S}$ was given in Section 2.4.

In order to describe the evolution of the vector $\mathbf{R}$ (or, equivalently, the inclination i and the longitude of the ascending node Ω), let us first deduce the equilibrium points of the problem.

Identification of the equilibrium points of the dynamical problem (27) is effectively a problem of eigenvalues and eigenvectors (see Allan and Cook (1964)). An equilibrium position of the problem (27), let us denote it by $\mathbf{V}$, is an eigenvector of the tensor $\omega_0\mathbf{R}_A\mathbf{R}_A + \omega_1\mathbf{R}_S\mathbf{R}_S$, that is

$$(\omega_0\mathbf{R}_A\mathbf{R}_A + \omega_1\mathbf{R}_S\mathbf{R}_S)\mathbf{V} = \lambda\mathbf{V},$$

where $\mathbf{AB}$ is the dyadic product of the vectors $\mathbf{A}$ and $\mathbf{B}$, and λ is an eigenvalue, that can be found by solving the algebraic equation

$$\det(\omega_A\mathbf{R}_A\mathbf{R}_0 + \omega_1\mathbf{R}_S\mathbf{R}_S - \lambda\mathbf{I}) = 0\,.$$

Here, $\mathbf{I}$ is the idemtensor.

It is easy to see that one eigenvalue is null, let us denote it by λ_1, $\lambda_1 = 0$, while the other two, namely λ_2 and λ_3 might be expressed in terms of the constants ω_0 and ω_1. Denoting by λ_2 and λ_3 the other two eigenvalues and considering that $\lambda_3 > \lambda_2 > \lambda_1$, we express them as it follows:

$$\begin{aligned}\lambda_1 &= 0,\\ \lambda_{2,3} &= \frac{1}{2}\Big(\omega_0 + \omega_1 \mp \sqrt{(\omega_0+\omega_1)^2 - 4\omega_0\omega_1\sin^2\epsilon}\Big),\end{aligned}$$

where $\epsilon = i_S^*$ is the obliquity, namely the angle between $\mathbf{R}_A$ and $\mathbf{R}_S$.

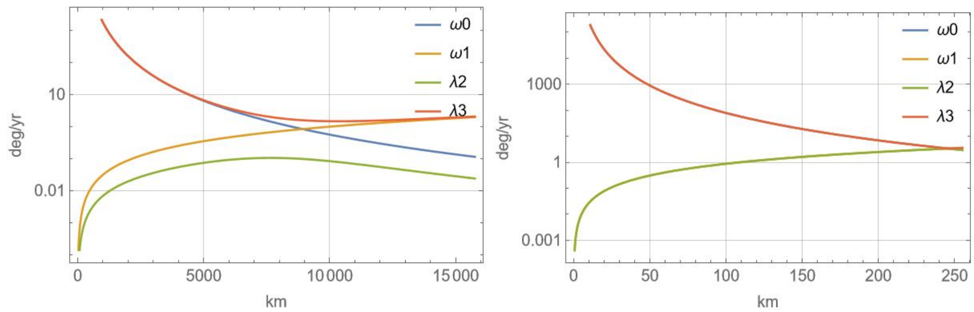

Fig. 3 – The values (in degrees/years) of ω_0, ω_1 and of the eigenvalues λ_2 and λ_3 for the cases of the asteroids Vesta (left) and Eros (right).

Figure 3 provides information on the rotational dynamics around the Vesta asteroid (left panel) and the Eros asteroid (right panel), respectively, showing the relationship between precession rates (ω_0, ω_1) and eigenvalues (λ_2, λ_3). In both cases, we can observe that the precession rate ω_0 dominates at smaller distances from the asteroid, while moving farther from it, ω_1 gains larger influence, highlighting the role of external gravitational forces.

The eigenvectors corresponding to the eigenvalues λ_1, λ_2, and λ_3, define the orientation of the principal axes, denoted in the following as O_1, O_2, and O_3, respectively. The axis O_3 is confined to the plane spanned by the polar axis of the asteroid ($\mathbf{R}_A$) and the normal to the Sun's orbital plane ($\mathbf{R}_S$), forming an inclination angle α relative to $\mathbf{R}_A$. This angle is determined by the relation (see Allan and Cook (1964)):

$$\tan 2\alpha = \frac{\omega_1 \sin 2\epsilon}{\omega_0 + \omega_1 \cos 2\epsilon}\,. \tag{28}$$

The axis O_1 is oriented orthogonally to the plane defined by $\mathbf{R}_A$ and $\mathbf{R}_S$, while O_2 resides within this plane and is orthogonal to O_3.

Because the unit vector $\mathbf{R}$ defines the orbital plane of the satellite P (namely the inclination i and the longitude of the ascending node Ω), knowing the motion of the vector $\mathbf{R}$ is equivalent to predicting the evolution of the orbital elements i and Ω. In fact, because the orbit remains circular and the semi-major axis is constant, one obtains the secular characterization of all elements.

The equilibrium solutions of (27), or equivalently, the equilibria in the (i,Ω) plane, lead to two types of motions of $\mathbf{R}$. Thus, the motion of the pole of the satellite's orbit **R** is constrained to lie on the unit sphere. The unit sphere is divided into two regions by a pair of bounding planes. These planes are determined by the eigenvalues (λ_1, λ_2, λ_3) of the system. The bounding planes separate the two regions where the pole **R** can move. The first region is defined for $\lambda_3 > \lambda_0 > \lambda_2$, when the pole **R** encircles the principal axis O_3. The second region appears in the case $\lambda_2 > \lambda_0 > \lambda_1$, when the pole **R** encircles the principal axis O_1.

The half-angle between the bounding planes is the angular separation between the two bounding planes and the principal axis O_3. Mathematically, it is denoted as $\frac{1}{2}\pi - \phi_2$, where ϕ_2 is the angle between the principal axis O_3 and the intersection of the trajectory with the plane O_1O_3. This angle determines the "width" of the regions on the unit sphere where the pole **R** can move.

The half-angle is related to the eigenvalues (λ_1, λ_2, λ_3) of the system. Specifically, the half-angle is determined by the ratio of the differences between the eigenvalues:

$$\tan(\phi_2) = \frac{\lambda_2 - \lambda_1}{\lambda_3 - \lambda_2}. \tag{29}$$

The relationship between the angle α (the angle between the principal axis O_3 and the asteroid's axis) and the half-angle $\frac{1}{2}\pi - \phi_2$ is determined by the geometry of the system and the eigenvalues (λ_1, λ_2, λ_3). Angle α affects the orientation of the principal axes, which in turn affects the eigenvalues and the semi-angle.

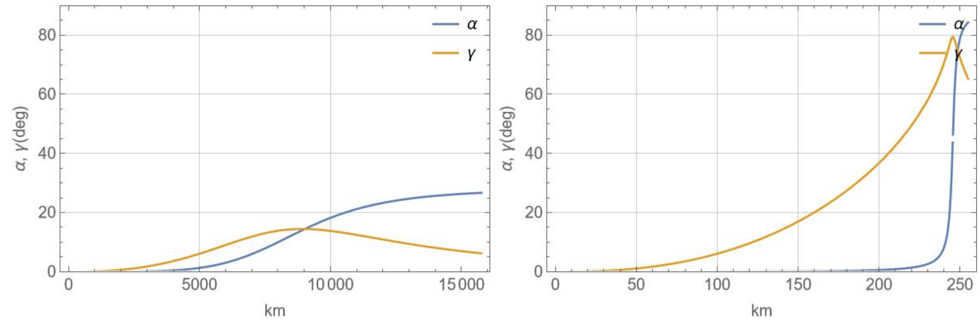

Fig. 4 – The evolution of the angle α and of the semi-angle $\gamma = \frac{1}{2}\pi - \phi_2$ for the cases of Vesta (left) and Eros (right).

Figure 4 shows the evolution of the angles α and γ and provides key information on the orbital and rotational dynamics around Vesta (left panel) and Eros (right panel). The increasing trend of α suggests a growing misalignment between the principal axis O_3 and a reference direction, with Vesta exhibiting a smoother transition due to its more centrally condensed moment of inertia, whereas Eros, with its elongated shape, introduces stronger perturbative effects in its vicinity (Chanut *et al.*, 2015).

The behavior of γ, defined as the half-angle $\frac{1}{2}\pi - \phi_2$, highlights the constraints on the rotational pole's motion. For Vesta, γ reaches a peak before decreasing around $40R_0$ (around 8 000 km), while for Eros, around $15R_0$ (around 250 km), marking a transition in the dominant dynamical effects. This peak corresponds to the region where the interaction between the gravitational asymmetry of the asteroid and the external torques is most significant (Scheidt *et al.*, 2016). The subsequent decline of γ at larger distances indicates a shift to a classical precession regime, where external forces, such as solar gravitational perturbations, become dominant (Fahnestock and Scheeres, 2008).

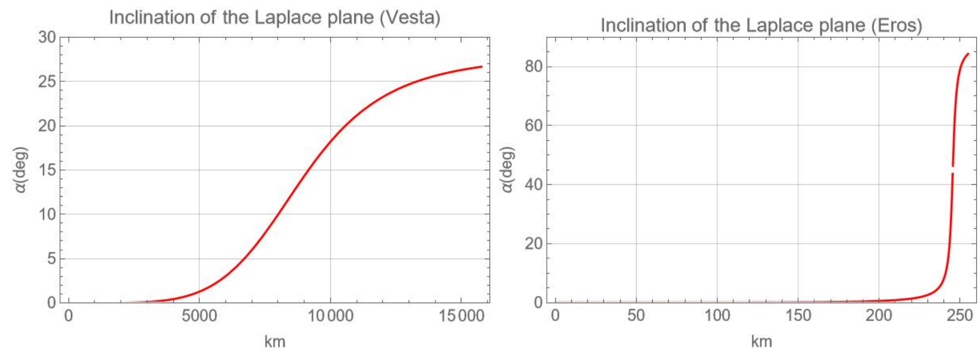

Fig. 5 – The location of the Laplace plane for the asteroids Vesta (left) and Eros (right).

As stated above, determining the equilibria of the system (27) is equivalent to solving an eigenvalue problem. Consequently, the dynamical system admits three equilibrium positions, corresponding to the alignment of the orbital plane with the principal axes. Two of these equilibria are stable, where the orbital plane aligns with either the equatorial plane of asteroid ($\mathbf{R}_A$) or the ecliptic plane ($\mathbf{R}_S$), while the third equilibrium is unstable, representing a saddle point configuration. As the normalized orbital distance increases, the angle α exhibits a monotonic increase, indicative of a progressive realignment of the principal axis O_3 away from the asteroid's polar axis.

At smaller distances, the stable equilibrium near $\mathbf{R}_A$ dominates, reflecting the strong influence of the asteroid's oblateness. However, as the distance increases, the stable equilibrium near $\mathbf{R}_S$ becomes increasingly significant, reflecting the growing influence of external perturbations.

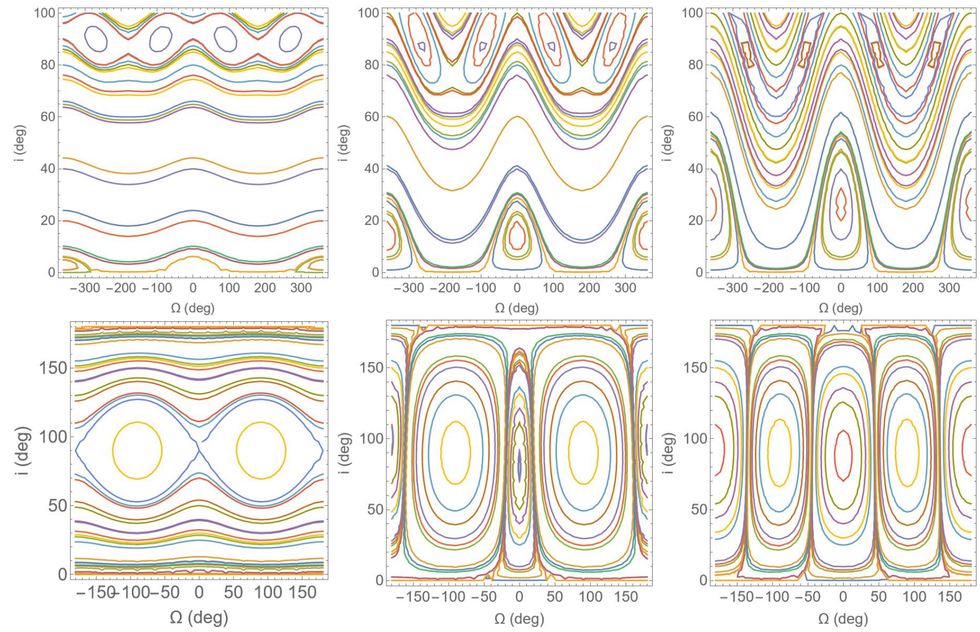

Fig. 6 – The level sets for the case of Vesta: a = 6 000 km (top left), a = 9 000 km (top middle), a = 15 000 km (top right). The level sets for the case of Eros: a = 200 km (bottom left), a = 250 km (bottom middle), a = 280 km (bottom right).

Within the (i, Ω) plane, the positions of these equilibrium points can be determined by analyzing the level sets of the Hamiltonian, as illustrated in Figure 6, in which two distinct cases are presented: the dynamics around Vesta, shown in the top panels, and the dynamics around Eros, depicted in the bottom panels. The level sets reveal that stable equilibria are characterized by closed contours, indicating regions of confined motion and orbital stability. In contrast, the unstable equilibrium is associated with open or distorted contours, signaling its sensitive dependence on initial conditions.

The amplitude of the librational islands is influenced by a variety of parameters, including the orbital elements of the Sun, the gravitational coefficient J_2, as well as the mass and shape of the asteroid. Among these parameters, asteroid's obliquity emerges as a key factor.

The obliquity, defined as the tilt of the asteroid's equatorial plane relative to its orbital plane, plays a crucial role in shaping the librational dynamics. To characterize this influence, we examined two distinct cases: Vesta, with an obliquity of $27°$ as reported by Tricarico and Sykes (2010) and Eros, which exhibits an obliquity of $89°$ according to Souchay *et al.* (2003). Our analysis indicates that the obliquity stands out as a fundamental parameter in understanding the structure and evolution of these librational regions, influencing both their width and their stability.

In the (i, Ω) plane, two types of motion can be distinguished, namely librational and rotational. The librational motion occurs when the system's trajectory remains confined around an equilibrium point, resulting in oscillations of the orbital elements within a bounded region of the phase space. On the other hand, rotational motion is characterized by the unbounded, monotonic variation of the angle Ω, as the trajectory encircles the phase space without confinement. The nature of these motions can be understood by integrating the vectorial equation (27), which can be reduced to a set of equations analogous to the Euler equations governing the motion of a rigid body. Through this reduction, the equilibrium positions, along with the amplitude of the librational islands, can be derived using the analytical formulas (28) and (29). These formulas provide a direct relationship between the orbital parameters and the gravitational harmonics, providing a theoretical framework to predict the behavior of the system without resorting to numerical simulations. The librational motion, in particular, is of significant interest, as it reflects the stability of the orbit.

Figure 6 presents the level sets for the Vesta case (at a = 6 000 km, a = 9 000 km and a = 15 000 km), top panels and for the Eros case (at $a = 200$ km, $a = 250$ km and $a = 280$ km), bottom panels. For orbital motions around Vesta, the level sets at a = 6 000 km exhibit well-defined contours, indicating three equilibrium positions near $(\Omega, i) = (0°, \alpha \approx 3°)$, $(0°, 90°)$, and $(90°, 90°)$, where external perturbative forces are small. As the semi-major axis increases to a = 9 000 km, or even larger to a = 15 000 km, the third-body perturbations increase in magnitude and, as a consequence, the inclination α of the Laplace plane tends to its maximum value of $27°$ (equal to the value of obliquity), while the width of librational islands increases.

For Eros, up to some distance, α is very small (as can be seen in the right panel of Figure 5, and the bottom left panel of Figure 6). But, with some larger values of a, since the obliquity is large, α suddenly increases up to $89°$ (see the bottom middle panel and the bottom right panel of Figure 6). As a consequence, the orbital inclination could exhibit high-amplitude excursions.

4. NUMERICAL SIMULATIONS

To validate the previous analytical analysis and to highlight the influence of the large excursions of the inclinations on the evolution of the other orbital elements, in particular the behavior of the eccentricity, we perform numerical simulations to propagate the orbits of an infinitesimal particle around the asteroids Vesta and Eros over extended time periods. We also highlight the role played by other perturbations, namely the effects induced by J_3 and the solar secular resonances. These simulations incorporate the gravitational harmonics of the asteroids, as well as perturbations due to the Sun.

Taking into account the effects of J_3, the initially circular orbits do not remain circular over time. Indeed, as effect of J_3, eccentricity varies according to the formula (see Galeş *et al.*, 2025):

$$\dot{e} = -\frac{3J_3\sqrt{\mu_0}R_0^3\Big(\sin(i)+5\sin(3i)\Big)\cos(\omega)}{32a^{9/2}\left(e^2-1\right)^2}\,. \tag{30}$$

On the other hand, third-body perturbations are responsible for the occurrence of secular resonances (see Hughes *et al.*, 1980). For orbits not very distant from the central body, the secular resonances depend only on the inclination and (for prograde orbits) are located at $i \approx 46^0$, $i \approx 56^0$, $i \approx 63.4^0$, $i \approx 69^0$, $i \approx 73^0$ and $i \approx 90^0$ (see Celletti *et al.*, 2016, 2017; Galeş *et al.*, 2025). The main effect of these resonances is the large variation of eccentricity. Thus, a non-circular orbit (even if the eccentricity is very small) might be located in the libration region of such a resonance and might experience large excursions in eccentricity.

Therefore, the mechanism that leads to large variations in eccentricity of initially circular orbits is the following: as effect of J_3, the eccentricity varies with small amplitudes; the coupled effect of J_2 and solar perturbations lead to large excursions in inclination. Once the inclination reaches a value equal to one of the critical values listed above, the orbit is influenced by a solar secular resonance and the eccentricity starts to increase.

The analytical results presented in the previous Section and the mechanism described above are confirmed by the Figures 7 and 8.

Figure 7 shows the orbital evolution of an infinitesimal particle around the asteroid Vesta for three cases: a = 6 000 km, a = 9 000 km and a = 15 000 km (while $e = 10^{-4}$ for all three situations). For all the situations the gravitational potential includes the harmonic terms J_2, J_3, and J_4, ensuring that the complex shape and mass distribution of Vesta are appropriately accounted for.

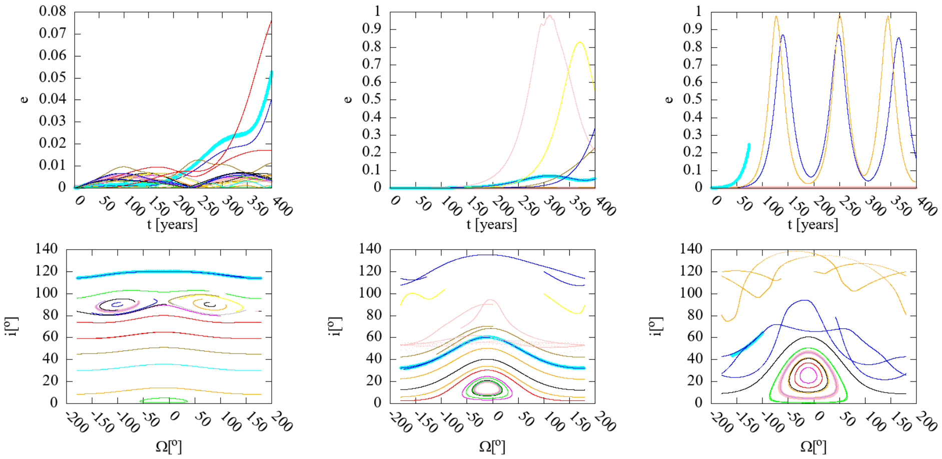

Fig. 7 – Evolution of the orbital elements for the case of a particle orbiting Vesta, located at the distances 6 000 km (left panels), 9 000 km (middle panels) and 15 000 km (right panels) with the initial eccentricity $e = 10^{-4}$. The pink and light blue thick lines represent orbits propagated using the Cartesian approach and the thin lines are obtained by using the Hamiltonian formalism (considering the harmonic terms J_2, J_3 and J_4).

All three panels illustrate the evolution of the eccentricity (e) depending on the time and the evolution of the plane inclination (i) - longitude of the ascending node (Ω). Both Cartesian and Hamiltonian approaches are used to propagate the orbits and the results show strong agreement, confirming the consistency and reliability of the two methods.

For a = 6 000 km, we can notice that the eccentricity is not significanlty increasing. Also in (i, Ω) plane, the dynamics is smooth, the librational islands are clearly illustrated.

For a = 9 000 km, the eccentricity variations become more significant, reaching up values close to 1 for some cases (when the inclination reaches a critical value associated to asolar secular resonance). In the (i, Ω) plane the behavior is still smooth enough.

At a = 15 000 km, the orbital dynamics become increasingly chaotic. The eccentricity undergoes large-amplitude oscillations, occasionally approaching values close to 1, indicative of potential orbital escape. Similarly, the inclination variations are more irregular, but the stability zones in the phase-space diagrams are still present.

Observational evidence suggests that Vesta does not currently host natural satellites, but the short-term stability zones identified in this analysis provide a theoretical framework for understanding transient orbital configurations.

Figure (8) shows the evolution of the orbital elements for the case of a particle orbiting Eros at $a = 200$ km, $a = 250$ km and $a = 280$ km (with the following initial eccentricity values: $e = 10^{-4}$ for the first case and $e = 10^{-6}$ for the latter two).

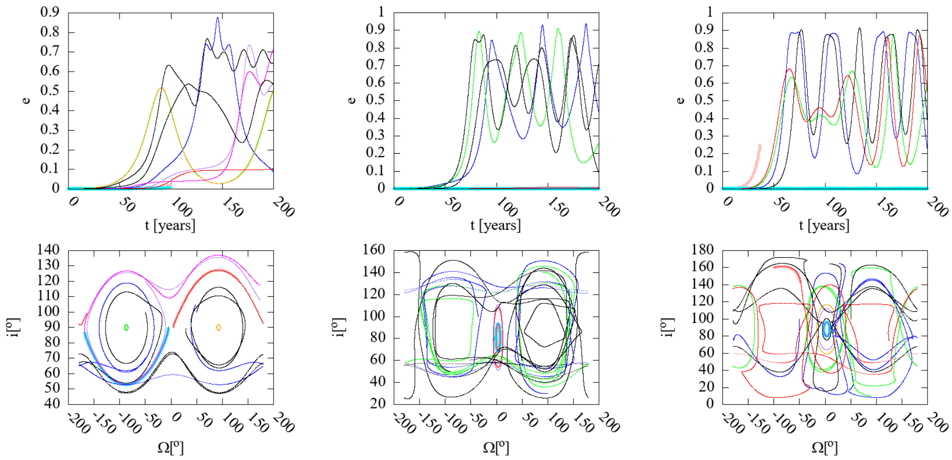

Fig. 8 – Evolution of the orbital elements for the case of particles orbiting Eros, located at the distances 200 km (left panels), 250 km (middle panels) and 280 km (right panels) with the initial eccentricity $e = 10^{-4}$ for the first case and $e = 10^{-6}$ for the latter two. The pink and light blue thick lines represent orbits propagated using the Cartesian approach (considering all 3 harmonic terms) and the thin lines are obtained by using the Hamiltonian formalism (considering also the three harmonic terms for $a = 200$ km and only the J_2 term for the latter two figures).

For $a = 200$ km, the considered orbits are located in the regions dominated by secular resonances, resulting in complex variations in eccentricity (e) over time. Eccentricity exhibits large oscillations, reaching values up to 0.8 during the integration period. The inclination shows coupled variations with the longitude of the ascending node (Ω), forming intricate phase-space trajectories.

For $a = 250$ km and $a = 280$ km, the orbital evolution becomes more chaotic. The eccentricity oscillates within wider bounds, reaching a maximum of 1. Inclination variations are also more unpredictable, with i and Ω following more complex and uneven trajectories.

A comparison of the three cases reveals a clear trend: as the semi-major axis increases, the orbital dynamics becomes chaotic. As noted above, even for small values of the semi-major axis, there exists a significant excursion of the eccentricity values. Therefore, there exists no certainty that a particle orbiting Eros remains around this asteroid. Consequently, Eros is not a suitable body to be able to possess companions.

5. CONCLUSIONS

The present paper presents a brief analysis of secular dynamics around asteroids with joint effects of oblateness and third body perturbations. Using both analytical and numerical tools, namely the Cartesian equations of motion, the Hamiltonian formalism and the Milankovitch elements, we studied the evolution of the orbital elements of various perturbed orbits around an oblate asteroid. Such an analysis provides the stability zones around an oblate body and the key parameters that influence the orbital regimes. Therefore, to identify the stable regions around an asteroid, we focused on the circular orbits.

Using a toy model, we presented an analytical study, which describes the long-term evolution of the orbital plane of a satellite orbiting an asteroid. We found that the evolution of inclination and longitude of the ascending node of satellite orbits depends on many parameters, such as the orbital elements of the asteroid, its density and shape, the zonal harmonics, the obliquity, etc. However, from this list, the parameter with the most relevant influence is obliquity. To underline this finding, our work investigates the dynamics around two relevant asteroids: (4) Vesta and (433) Eros, because of their different obliquity. Vesta's obliquity is approximately $27°$, while Eros's obliquity is $89°$. At farther and farther distances from the asteroid with a large obliquity, the width of librational regions in the (i, Ω) plane increases, leading to larger and larger excursions of the inclination (see the bottom panels of Figure 6).

The analytical results are then validated by numerical studies by considering more complete models that take into account additional harmonics, in particular, the J_3 term. It is known that the J_3 perturbations induce variations of the eccentricity. Although these are small, initially circular orbits will not remain circular. If at some time the inclination reaches a value corresponding to a secular solar resonance (depending only on inclination, see Celletti *et al.*, 2020), the orbiting particle is influenced by this resonance. The main effect of secular resonances is the large variation of eccentricity. So, as long as the orbital inclination does not reach a value corresponding to a secular resonance, the orbit remains stable in the sense that the eccentricity does not increase over time. Otherwise, when the inclination undergoes large excursions, the eccentricity could not remain small once a secular resonance is reached.

We may conclude that Vesta could possess some companions (satellites or infinitesimal particles) even at large distances from its surface, as long as the inclination is smaller than about $40°$. The reason is that the solar secular resonances (depending only on the inclination) occur at inclinations larger than $45°$ and the inclination does not increase over time (as described in Section 3).

However, in the case of Eros, the existence of companions is impossible at large distances, let say at distances larger than 250 km (see the bottom plots of Figure 6), because the inclination of each orbit will reach at some time the inclination of a secular solar resonance.

Acknowledgements. Acknowledgment is given to infrastructure support from the Operational Program Competitiveness 2014-2020, Axis 1, under POC/448/1/1 Research infrastructure projects for public R&D institutions/Sections F 2018, through the Research Center with Integrated Techniques for Atmospheric Aerosol Investigation in Romania (RECENT AIR) project, under grant agreement MySMIS no.127324.

REFERENCES

Allan R.R., and Cook G.E.: 1964, *Proc. R. Soc. Lond. A* **280**, 97.

Archinal B.A., A'Hearn M.F., Bowell E., Conrad A., Consolmagno G.J., Courtin R., Fukushima T., Hestroffer D., Hilton J.L., Krasinsky G.A., Neumann G., Oberst J., Seidelmann P.K., Stooke P., Tholen D.J., Thomas P.C., and Williams I.P.: 2011, Report of the IAU Working Group on Cartographic Coordinates and Rotational Elements: 2009, *Celest. Mech. Dyn. Astr.*, **109**, 101.

Bills B.G., and Nimmo F.: 2011, *Icarus*, **213**(2), 496.

Brouwer D., and Clemence G.M.: 1961, Methods of Celestial Mechanics, *Academic Press*.

Cavallari I., Grassi C., Gronchi G.F., Baù G., and Valsecchi G.: 2023, **119**, 107091.

Celletti A., Gales C., Pucacco G.: 2016, *SIAM Journal on Applied Dynamical Systems*, **15**, 1352.

Celletti A., Gales C., Pucacco G., and Rosengren A.: 2017, *Celestial Mechanics and Dynamical Astronomy*, **127**, 259.

Celletti A., Galeş C., Lhotka C.: 2020, *Communications in Nonlinear Science and Numerical Simulation*, **84**, 105185.

Chanut T.G.G., Winter O.C., and Tsuchida M.: 2015, *Monthly Notices of the Royal Astronomical Society*, **450**(4), 3742.

Fahnestock E.G., and Scheeres D.J.: 2008, *Icarus*, **194** (2), 410.

Galeș C., Nadabaică G., and Apertii M.: 2025, *Preprint submited for publication.*

Giacaglia G.E.O.: 1976, *Celestial Mechanics*, **14**, 515.

Hughes, S.: 1980, *Proc. R. Soc. Lond. A*, **372**, 243.

Kaula W.M.: 1961, *Geophysical Journal International*, **5**(2), 104.

Kaula W.M.: 1962, *Astronomical Journal*, **67**, 300.

Kaula W.M.: 1966, *Blaisdell, Waltham*.

Konopliv A.S., Park R.S., Asmar S.W., and Buccino D.R.: 2017, *NASA Planetary Data System, DAWN-A-RSS-5-VEGR-V2.0*

Milankovitch M.: 1939, *Bull. Acad. Sci. Math. Nat. A*, **6**, 1.

Miller J.K., Konopliv A.S., Antreasian P.G., Bordi J.J., Chesley S., Helfrich C.E., Owen W.M., Wang T.C., Williams B.G., Yeomans D.K., and Scheeres D.J.: 2002, *Icarus*, **155**, 3.

Murray C.D., and Dermott S.F.: 1999, *Cambridge University Press*.

Russell C.T., et al.: 2012, *Science*, **336**(6082), 684-.

Scheeres D.J., et al.: 2000, *Journal of the Astronautical Sciences*, **48**(1), 35.

Scheeres D.J.: 2012, *Springer*.

Scheidt R.A., et al.: 2016, *Celestial Mechanics and Dynamical Astronomy*, **124**(3), 275.

Souchay J., Kinoshita H., Nakai H., and Roux S.: 2003, *Icarus*, **166**, 285.

Tricarico P., and Sykes M.V.: 2010, *Planetary and Space Science*, **58**, 1516.

Received on 15 March 2025